Chemical Tailoring of Porous Silica Xerogels: Local Structure by Vibrational Spectroscopy

Alexandra Fidalgo and Laura M. Ilharco*[a]

Abstract: Monolithic porous silica xerogels were synthesized by the sol–gel process, and their local structure was analysed by vibrational spectroscopy. The silica alcogels were prepared by a two-step hydrolytic polycondensation of tetraethoxysilane (TEOS) in isopropanol, with a water/TEOS molar ratio of 4. The hydrolysis step was catalysed by hydrochloric acid (HCl), with different HCl/TEOS molar ratios (ranging from 0.0005 to 0.009), and the condensation step was catalysed by ammonia (NH_3), with different NH_3/HCl molar ratios (ranging from 0.7 to 1.7). After appropriate ageing, the alcogels were washed with isopropanol and subcritically dried at atmospheric pressure. The diffuse reflectance infrared Fourier transform (DRIFT) spectra were analysed in terms of the main siloxane rings that form the silica particles, taking into account the splitting of the ν_{as}Si–O–Si mode into pairs of longitudinal and transverse optic components, by long-range Coulomb interactions. It was proven that the proportion of residual silanol groups (which correlates with hydrophilicity), and the fraction of siloxane 6-rings (which correlates with porosity) may be tailored by adequate catalytic conditions, mostly by the hydrolysis pH. This was explained in terms of the reactions' mechanisms taking place in the two-step sol–gel process followed.

Keywords: hydrophobicity · IR spectroscopy · silicon · siloxane rings · sol–gel processes

Introduction

The sol–gel process consists basically of the synthesis of an amorphous inorganic network by chemical reactions in solution at low temperature. The most prominent feature of this process, the transition from a liquid (solution or colloidal solution) into a solid (di- or multiphasic gel) led to the expression "sol–gel process".[1] Any molecule able to undergo hydrolysis and polycondensation reactions, and, therefore, to form reactive "inorganic" monomers or oligomers, can be used as a precursor for sol–gel techniques.[2] Nevertheless, most work in the sol–gel field has been performed with metal alkoxides as precursors, since they provide a convenient source for "inorganic" monomers, with the advantage of being soluble in common organic solvents. Another advantage of the alkoxide route is the possibility to control hydrolysis and condensation kinetics by solution chemistry, rather than by surface or colloidal chemistry. In solution, the alkoxides are hydrolysed and condensed into polymeric species composed of metal–oxygen–metal bonds.[3] At the functional group level, three reactions are generally used to describe the sol–gel process, as shown bellow for silicon alkoxides, $Si(OR)_4$ [Eqs. (1)–(3)]:[4]

$$(RO)_3Si{-}OR + H_2O \underset{\text{esterification}}{\overset{\text{hydrolysis}}{\rightleftharpoons}} (RO)_3Si{-}OH + ROH \quad (1)$$

$$(RO)_3Si{-}OH + RO{-}Si(OR)_3 \underset{\text{alcoholysis}}{\overset{\text{alcohol condensation}}{\rightleftharpoons}} (RO)_3Si{-}O{-}Si(OR)_3 + ROH \quad (2)$$

$$(RO)_3Si{-}OH + HO{-}Si(OR)_3 \underset{\text{hydrolysis}}{\overset{\text{water condensation}}{\rightleftharpoons}} (RO)_3Si{-}O{-}Si(OR)_3 + H_2O \quad (3)$$

It is clear from the above equations that the structure of sol–gel materials evolves sequentially, being the product of successive and/or simultaneous hydrolysis, condensation and their reverse reactions (esterification and depolymerization). Thus, by chemical control of the mechanisms and kinetics of these reactions, namely the catalytic conditions, it is possible to tailor the structure and properties of the gels over a wide range.

Actually, these reactions never result in the formation of pure oxides,[5] and the overall hydrolytic polycondensation reaction can be written as Equation (4):[6]

$$n\mathrm{Si(OR)_4} + m\mathrm{H_2O} \rightarrow \mathrm{Si}_n\mathrm{O}_{2n-(a+b)/2}(\mathrm{OH})_a(\mathrm{OR})_b + (4n\text{-}b)\mathrm{ROH} \quad (4)$$

[a] A. Fidalgo, Prof. L. M. Ilharco
Centro de Química-Física Molecular
Complexo I, Instituto Superior Técnico
Av. Rovisco Pais 1
1049–001 Lisboa (Portugal)
Fax: (+351) 21–8464455
E-mail: lilharco@ist.utl.pt

DOI: 10.1002/chem.200305079

in which $m=2n+(a-b)/2$. The resulting gel is chemically unstable, since its alkoxy (OR) groups are subject to further hydrolysis by the presence of unreacted water. Consequently, the dry gel (xerogel) obtained by removal of the residual solvent is also unstable, since the remaining hydroxyl (OH) groups can further condense by exposure to moisture. The net result is a "living" material that undergoes structural modifications, even months after preparation.

Usually, any attempt to reduce the concentration of OR and OH terminal groups, either by changing the reaction parameters or by thermal treatment of the xerogel, resulted in a dramatic reduction of porosity.[6] This severely limits the range of applications of xerogels, namely when high porosity is required. Recently, we have shown the possibility of producing rather stable silica xerogels with increased porosity, by a tight control of the hydrolysis and condensation catalytic conditions in a two-step sol–gel process.[7] This is a modification of the two-step method developed by Brinker et al.,[8,9] and allows increasing the overall yield of silica production by an efficient separation of the hydrolysis and condensation mechanisms. The silicon alkoxide is firstly hydrolysed in a strong acidic medium, at such pH values that condensation reactions are very slow,[10] according to the following mechanism given in Equations (5) and (6):[1]

$$Si(OR)_4 + H^+ \overset{\text{fast}}{\rightleftharpoons} (RO)_3Si-(ORH)^+ \quad (5)$$

$$(RO)_3Si-(ORH)^+ + H_2O \overset{\text{slow}}{\rightleftharpoons} HO-Si(OR)_3 + ROH + H^+ \quad (6)$$

in which R is an alkyl group or a hydrogen atom. The sol is then neutralised to promote the condensation reaction under a base catalysed mechanism, as shown in Equations (7) and (8):[8]

$$(RO)_3Si-(OH) + HO^- \overset{\text{fast}}{\rightleftharpoons} (RO)_3Si-O^- + H_2O \quad (7)$$

$$(RO)_3Si-O^- + HO-Si(OR)_3 \overset{\text{slow}}{\rightleftharpoons} (RO)_3Si-O-Si(OR)_3 + OH^- \quad (8)$$

in which $R \equiv H$ or $Si(OR)_3$. Within this two-step process, at the onset of condensation there are mostly hydroxyl groups bonded to silicon; this favours cross-linking. Furthermore, the base-catalysed polymerisation mechanism also favours cross-linking, since the extension of Equation (7) increases with the Si–OH acidity, which is stronger for the already more cross-linked clusters. The net result is that the larger polymers grow at expense of the smaller ones, originating a highly cross-linked gel, which is essentially pure silica.[8,9]

By tuning the acid and base contents in each step, we were able to tailor the particle dimensions, pore morphology, density and porosity of the silica xerogels, from relatively dense to highly porous ones.[7] Such drastic changes in morphology and physical properties must be correlated to structural modifications at molecular level. Vibrational spectroscopy, in particular diffuse reflectance infrared Fourier transform spectroscopy (DRIFT), has already proven very valuable to characterise silica xerogels, providing information on the structural units, porosity, residual silanol groups (that determine the gels' hydrophilicity) and other structural defects.[11–13] As the present paper aims to correlate structural with macroscopic characteristics of the gels, a brief review of the state of the art on this matter will follow.

The fundamental structural units of silica gel are similar to those of vitreous silica and the vibrational features may be explained accordingly. The starting point for interpreting the vibrational spectra of AX_2 glasses was the central force-field model proposed by Sen and Thorpe,[14] and later developed by Galeener.[15] Bearing in mind the long-accepted structure of these glasses (a continuous random network of nearly perfect AX_4 tetrahedral units[16]), the central force model assumes that the local order of the basic tetrahedra is largely retained, and only takes into account the nearest-neighbour central force between A and X atoms. Since the noncentral force constants (such as angle bending) are generally small, this simplification is satisfactory for representing high-frequency (i.e. A–X stretching) vibrational modes. The A–X–A coupling angle between tetrahedra (θ, in Figure 1) may vary between 90° and 180°, and determines to a large extent the importance of the collective effects.

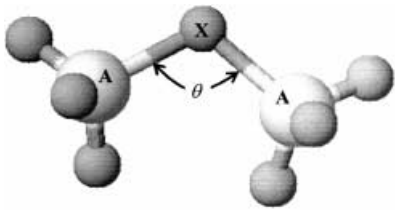

Figure 1. Schematic diagram of the local order assumed for AX_2 glasses, showing two AX_4 units and the intertetrahedral angle, θ.

For $\theta=90°$, the effective coupling between neighbouring tetrahedra is zero, and the two high-frequency modes of an isolated AX_4 unit (namely a totally symmetric singlet, A_1, and an antisymmetric triplet T_2) retain the molecular-like character. As θ increases, so does the coupling, and those vibrational modes become extended band-like solid-state ones, as a consequence of the bonding and antibonding bands emerging from sp^3-hybridized atomic orbitals. There is a critical angle, θ_c, above which the solid-state effects predominate.[14] In the case of glassy SiO_2, θ has a fairly broad distribution of values (estimated to lie between 120° and 180°), with a maximum at ~140°,[17] and θ_c was found to be 117°.[18] As a result, $\theta > \theta_c$, which means that the solid-state effects take over and so the high-frequency modes are band-like. This model allowed the calculation of the bands' limiting frequencies as a function of θ, according to Equations (9)–(12):

$$\omega_1^2 = (\alpha/M_O)(1 + \cos\theta) \quad (9)$$

$$\omega_2^2 = (\alpha/M_O)(1-\cos\theta) \quad (10)$$

$$\omega_3^2 = (\alpha/M_O)(1 + \cos\theta) + (4\alpha/3M_{Si}) \quad (11)$$

$$\omega_4^2 = (\alpha/M_O)(1-\cos\theta) + (4\alpha/3M_{Si}) \quad (12)$$

in which the pairs (ω_1,ω_2) and (ω_3,ω_4) are the edge-angular frequencies of the two high-frequency bands, α is the central force constant, and M_O and M_{Si} are the atomic masses of oxygen and silicon.[14] This model was later extended to account for the presence of small, planar rings, improving the agreement between the calculated bands limits and the experimental results,[19] as all network glasses contain complete rings of bonds. For vitreous silica, for instance, the interpretation of the sharp Raman bands D_1 and D_2, at 495 and 606 cm^{-1}, respectively, led to considering the existence of both siloxane 3- and 4-rings (rings containing three and four silicon atoms, respectively).[20] For silica gels, it was proposed that the tetrahedral units are mostly arranged in siloxane 4-rings, which are thermodynamically favoured, not excluding the presence of less tensioned 6-rings, which are kinetically favoured.[1,21,22] The analysis of the vibrational spectra of disordered solids was not complete without the inclusion of long-range interactions, provided by Coulomb fields associated with certain excitations of the system.[23,24] For crystalline solids, the effect of Coulomb forces on the phonon dispersion curves was well known in the late 1970 s:[25] in the absence of retardation effects and when the wave vector of the incoming light (**k**) is zero, there is a splitting of the optical modes into a pair of longitudinal-optic (LO)/transverse-optic (TO) components. For glasses, although experimental evidence pointed to LO–TO splitting,[23] the theoretical problem was solved somewhat later, since disordered solids have no microscopic translational invariance and so the wave vector **k** is no longer a good internal quantum label. For AX_2 random networks, the equation of motion technique was used to give numerical evidence of the LO–TO splitting,[26] yielding a splitting of 140 cm^{-1} for the highest frequency mode in vitreous silica, only slightly less than the experimental value for α-quartz (~163 cm^{-1}).[24]

In summary, for silica gels, it is expected that the high-frequency infrared-active antisymmetric stretch Si–O–Si will appear in the DRIFT spectra as a broad band, with limiting frequencies determined roughly by the central force model for each coupling angle. Specific band-limiting frequencies will arise for each population of ring dimensions, since they correspond to different average coupling angles. Moreover, these bands will be split in two components (LO–TO), more or less clearly separated, depending on the degree of long-range interactions in the sample. It is the purpose of the present work to use the information from DRIFT spectra to highlight the local structural changes imparted in xerogels by the chemical tailoring of their porous structure.

Experimental Section

Materials: The silica sols were prepared by using tetraethoxysilane (TEOS) from Alpha Products (99 % pure) as the silica source, 2-propanol (*i*PrOH) from Riedel-de Haën (reagent grade) as solvent, and distilled-deionised water. The catalysts used in the hydrolysis and condensation steps were HCl (from Riedel-de Haën, 1N) and NH_3 (from Merck, 33 %, diluted to 0.1 N), respectively.

Xerogels preparation: The silica alcogels were synthesized, aged and dried following the procedure schematised in Figure 2.

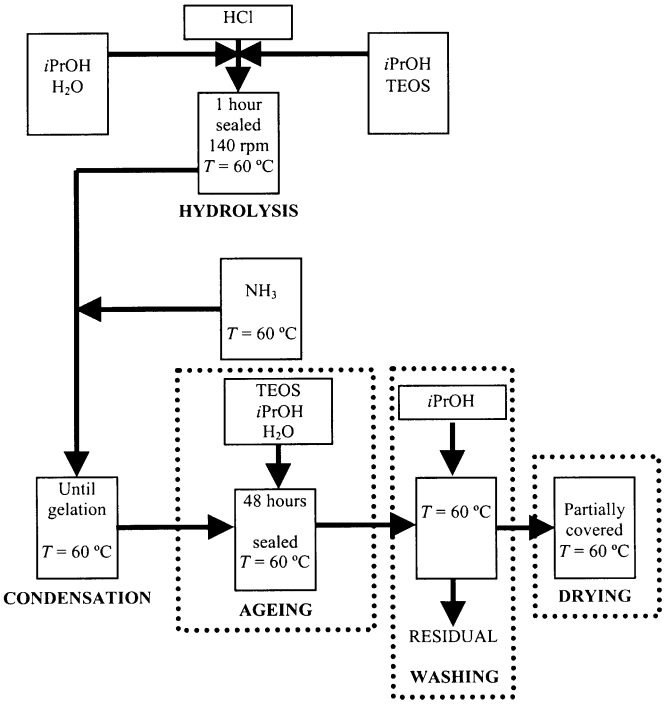

Figure 2. Schematic representation of the sample preparation procedure.

TEOS was first diluted in half the amount of solvent. The remaining solvent was mixed with water and added dropwise to the TEOS mixture, under vigorous stirring. The reaction mixture was then acidified with the required amount of HCl and its pH measured, without correction for a nonaqueous medium. The acidic sol was placed in a high density polypropylene sealed container, heated at 60 °C and stirred (140 rpm) for 60 minutes. The required amount of NH_3 was then added, and the resulting homogeneous sol was left to gel, with no further stirring, in the sealed containers at 60 °C. To strengthen the silica network, the alcogels were aged for 48 h at 60 °C: the first 24 h in the residual liquid, and the latter in an ageing solution that contained TEOS, *i*PrOH, and H_2O in the same proportions as used for the alcogels synthesis (the volume of added ageing solution was equal to the initial sol volume). The pore liquid was then exchanged with *i*PrOH to completely remove any residual water or TEOS and the washed gels were dried at 60 °C under ambient pressure, partially covered, until the weight loss became negligible. Following this general procedure, two sets of alcogels were prepared with molar compositions $TEOS/H_2O/iPrOH$ 1:4:9.2, and different HCl/TEOS (x) and NH_3/HCl (y) molar ratios, x ranging from 0.0005 to 0.009 and y from 0.7 to 1.7. The samples were identified as HYD_{1000x} and $COND_{10y}$, as indicated in Table 1.

Table 1. Sample identification in terms of the molar ratios x (HCl/TEOS) and y (NH_3/HCl).

Sample	x	Hydrolysis pH	y
$HYD_{0.5}$	0.0005	2.75	1.0
HYD_1	0.001	2.45	1.0
HYD_3[a]	0.003	1.88	1.0
HYD_5	0.005	1.71	1.0
HYD_7	0.007	1.54	1.0
HYD_9	0.009	1.36	1.0
$COND_7$	0.003	1.88	0.7
$COND_{10}$[a]	0.003	1.88	1.0
$COND_{13}$	0.003	1.88	1.3
$COND_{17}$	0.003	1.88	1.7

[a] Samples HYD_3 and $COND_{10}$ are equivalent, and were prepared for reproducibility check.

Sample characterisation: The molecular structure of the xerogels was analysed by diffuse reflectance infrared Fourier transform (DRIFT) spectroscopy, by using a Mattson RS1 FTIR spectrometer with a Specac Selector, in the range 4000–400 cm^{-1} (wide band MCT detector), at 4 cm^{-1} resolution. The spectra were the result of 100 added scans for each sample, ratioed against the same number of scans for the background (ground KBr, FTIR grade, from Aldrich). The sample preparation for DRIFT analysis consisted simply in grinding a mixture of KBr and xerogel, in appropriate weight proportions, to obtain spectral absorbance in the range of applicability of the Kubelka–Munk transformation.[27]

Results and Discussion

Molecular structure: The DRIFT spectra of selected dried samples are shown in Figure 3A (HYD series) and Figure 3B (COND series). The spectra were normalised to the most intense absorption band, the ν_{as}Si–O–Si mode, at ~1090 cm^{-1}, to allow comparing the band intensities relative to the silica network.

They were interpreted taking into account that the elementary SiO_4 units are arranged mostly in siloxane 4- $(SiO)_4$ and 6-rings $(SiO)_6$, as schematized in Figure 4.

Structural defects such as dangling oxygen atoms (residual Si–OH and Si–O^- groups) were also taken into account, but other defects like smaller and larger siloxane rings were neglected. The broad band centred at ~3400 cm^{-1} is assigned to the O–H stretching mode of silanol groups and water (residual and/or adsorbed), involved in a variety of hydrogen bonds. The presence of adsorbed water, although in trace amounts for some samples, is confirmed by the corresponding deformation band at ~1640 cm^{-1}. The bands at 950 and 800 cm^{-1} are assigned to the dangling Si–O ($\tilde{\nu}$Si–O_d) and the symmetric Si–O–Si ($\tilde{\nu}_s$Si–O–Si) stretching modes, respectively. A small but distinct feature is observed at ~560 cm^{-1} in all the spectra. It has been correlated by Kamiya et al.[28] and Yoshino et al.[29] to siloxane 4-rings, and was lately assigned, by molecular orbital calculations, to the 4-ring vibration within the ring plane that results from the coupling of the Si–O stretching to the O–Si–O and Si–O–Si bending modes.[30] The band assignments proposed for the DRIFT spectra are indicated in Table 2.

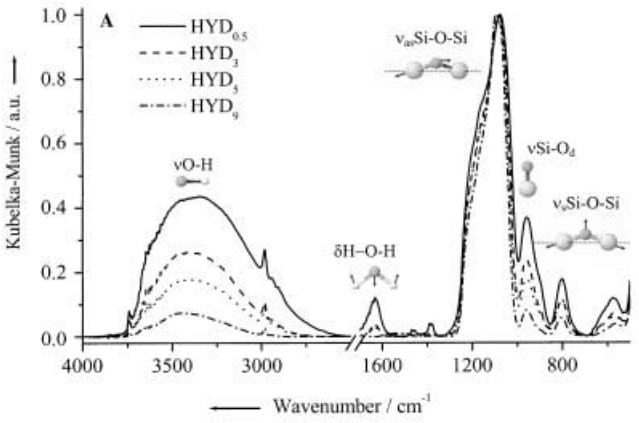

Figure 3. DRIFT spectra of selected samples with different x (A) and y (B) molar ratios. The spectra were normalised to the maximum of the ν_{as}Si–O–Si band.

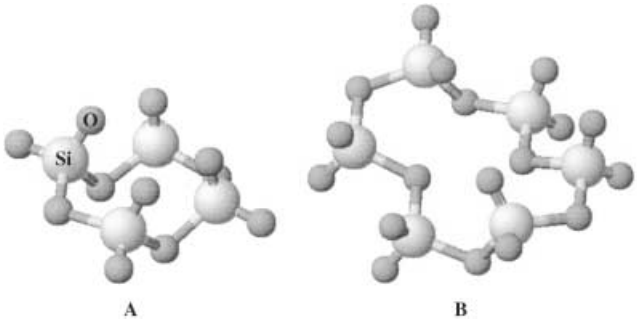

Figure 4. Schematic diagram of the more common types of primary cyclic arrangements of the structural units, SiO_4, in xerogels: A) 4-ring $(SiO)_4$ and B) 6-ring $(SiO)_6$ siloxane.

In the spectra of HYD samples (Figure 3A), there is a gradual decrease of the bands at ~3400, 1640 and ~950 cm^{-1} with increasing molar ratio x (decreasing hydrolysis pH), reflecting the decrease in the relative amounts of residual silanol groups and adsorbed water. Therefore, more hydrophobic materials are obtained by increasing the HCl/TEOS molar ratio. This is consistent with a higher overall yield of silica production, resulting from a larger hydrolysis extent at the moment of ammonia addition. For COND samples (Figure 3B), the same trend is observed with increasing y, showing that the condensation extent of sols with equivalent hydrolysis conditions is determined by the NH_3/HCl ratio, and also influences the xerogels' hydrophobicity. Since the evolution is clearer for HYD samples, the following detailed analysis will concern their spectra. Besides the decrease of the silanol related bands, there is an evident

Table 2. Band assignments of the DRIFT spectra in Figure 3.

Wavenumber [cm^{-1}]	Assignment
3800–2500	νO–H (H_2O + SiO–H)
~1640	δH–O–H (H_2O)
~1090	ν_{as}Si–O–Si (4- + 6-rings)
950	νSi–O_d (Si–OH and Si–O^-)
800	ν_sSi–O–Si (4- + 6-rings)
560	νSi–O coupled with δO–Si–O and δSi–O–Si (in 4-rings)

modification in the ν_{as}Si–O–Si band shape, showing that a slight adjustment in the hydrolysis pH (from 2.75 to 1.36) is responsible for structural changes in the silica network as well. Additionally, there is a parallel decrease in the feature at 560 cm^{-1}, suggesting that these structural changes are associated to a reduction of the proportion of 4-rings.

To quantify the preceding analysis, a deconvolution of the spectral region between 1350 and 700 cm^{-1} was performed by a nonlinear least squares fitting method, by means of Gaussian functions. The deconvolution profiles obtained for the spectra in Figure 3A are shown in Figure 5, superimposed with the experimental results (dotted lines).

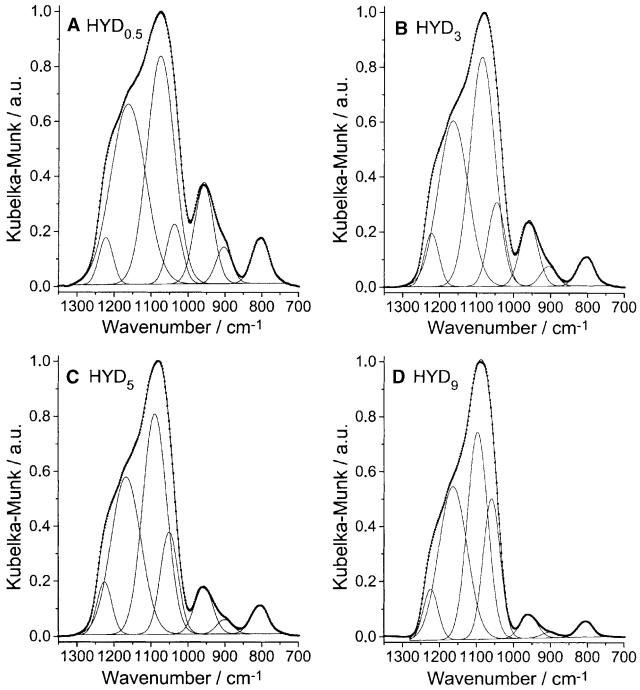

Figure 5. Deconvolution of the spectral region between 1350 and 700 cm^{-1} for selected samples with different HCl/TEOS molar ratios. The dotted lines correspond to the experimental spectra.

The best fit for the ν_{as}Si–O–Si band was obtained with four Gaussians, with maxima at around 1220, 1160, 1080 and 1050 cm^{-1}. These components must reflect the populations of $(SiO)_6$ and $(SiO)_4$ units in the silica backbone structure, and their assignments depend on a number of assertions:

1) The 4-rings are more tensioned, with $\theta \approx 125°$, than the 6-rings, with $\theta \approx 140°$.[31] Using these average values for θ, and bearing in mind that $\theta > \theta_c$ for both ring types,[18] the limiting frequencies of the ν_{as}Si–O–Si bands can be estimated by the simplified central force-field model, Equations (11) and (12), resulting broader in the case of 6-rings (lower ω_3 and higher ω_4).
2) The expected LO–TO splitting due to long-range interactions is of the order of 140 to 160 cm^{-1} for 6-rings.[24,26]
3) The 4-rings are expected to be predominant in silica gels.[1]

All these remarks point to the following tentative assignments: the dominant and closer components, at ~1160 and ~1080 cm^{-1}, correspond to the LO–TO pair of siloxane 4-rings, and the minor and more apart ones, at ~1220 and ~1050 cm^{-1}, to the LO–TO pair of 6-rings.

The quantitative results of the ν_{as}Si–O–Si band deconvolution are summarized in Table 3 for all the samples. While the position of the LO modes is almost insensitive to the catalytic conditions, there is a clear shift of the TO components to higher wavenumbers with increasing x and y. Consequently, the LO–TO splitting decreases for both ring types, in a good indication that the long-range Coulomb interactions are reduced, probably due to a larger distance between interacting species, associated with a higher porosity.[7] There are also net variations of the percentual areas with the ratios x and y: with increasing x, the relative areas related to the 4-ring units decrease (LO from 44.5 to 37.1% and TO from 44.1 to 36.1%), whereas those related to 6-ring units increase (LO from 5.7 to 6.4 and TO from 6.6 to 20.4%). The same trend is observed when y increases up to 1.3 (sample $COND_{13}$). Since both the positions and percentual areas of the TO modes are more sensitive to the hydrol-

Table 3. Main results of the deconvolution of the ν_{as}Si–O–Si band in Gaussian components for all the samples.[a]

		$HYD_{0.5}$	HYD_1	HYD_3	HYD_5	HYD_7	HYD_9	$COND_7$	$COND_{10}$	$COND_{13}$	$COND_{17}$
LO $(SiO)_6$	$\tilde{\nu}$	1222	1220	1222	1226	1224	1223	1220	1224	1224	1223
	W	45	46	46	47	47	47	45	44	45	46
	%A	4.7	5.4	6.1	6.2	6.9	6.4	5.3	4.8	5.7	6.0
LO $(SiO)_4$	$\tilde{\nu}$	1163	1162	1163	1167	1166	1163	1162	1164	1165	1165
	W	110	101	94	94	88	90	100	105	94	90
	%A	44.5	40.9	38.6	37.2	31.7	37.1	40.6	42.6	37.3	35.9
TO $(SiO)_4$	$\tilde{\nu}$	1075	1077	1084	1089	1091	1097	1076	1083	1092	1090
	W	86	85	78	76	74	64	83	77	72	75
	%A	44.1	46.1	44.1	42.3	43.7	36.1	49.3	40.4	37.2	44.8
TO $(SiO)_6$	$\tilde{\nu}$	1037	1037	1046	1051	1058	1058	1036	1045	1053	1054
	W	50	52	54	56	53	54	49	56	59	55
	%A	6.6	7.6	11.2	14.4	14.4	20.4	4.8	12.1	19.9	13.2
$\%(SiO)_6$		11	13	17	20	21	27	10	17	26	19

[a] $\tilde{\nu}$: wavenumber of maximum absorption [cm^{-1}]; W: full width at half maximum [cm^{-1}]; %A: percentual area.

ysis and condensation pH values, the bare modes (the intrinsic vibrations that are decoupled) must be closer to this optic component, as pointed out by other authors.[24]

The percentages of 6-ring units in the silica network, $\%(SiO)_6$, are listed in the last row of Table 3, and were obtained simply by adding $\%A[LO(SiO)_6]$ and $\%A[TO(SiO)_6]$. There is a clear increase in the $\%(SiO)_6$ with x, and with y up to a value of 1.3. These results relate perfectly with the prior evidence of a decrease in the proportion of $(SiO)_4$ units, given by the evolution of the 560 cm^{-1} band, and confirm the assignment of the ν_{as}Si–O–Si components.

Also worthy of mention in Table 3 are the full-widths at half maximum of the optic components (W): those of $(SiO)_6$ units (both LO and TO) are almost invariant, while those of $(SiO)_4$ rings are large and decrease systematically with increasing x and y. This may be ascribed to a local ordering of the $(SiO)_4$ population, accompanied by a narrowing in the statistical distribution of coupling angles. Such evolution must be related to a direct formation of 4-rings with increasing x (more extensive hydrolysis prior to condensation), instead of resulting from network relaxation processes involving 6- to 4-ring conversion.[22]

From the preceding analysis, it follows that the siloxane 4-rings are predominant in all the xerogels prepared. Decreasing the hydrolysis pH and/or increasing the NH_3/HCl ratio leads to an increase in the proportion of 6-rings (up to ~30% for the pH range explored) and, therefore, to a more three-dimensional, glass-like structure,[32] although more porous.[7]

Degree of hydrophobicity: Given that all silica xerogels contain small mesopores, moisture condensation in the pores may lead to the collapse of the silica structure by capillary forces. However, some of the samples prepared in the present work revealed a certain degree of hydrophobicity (mainly those with higher x and y ratios). This was concluded from the observed decrease in the silanol related bands with increasing molar ratios x and y, and can be quantified by deconvolution of the band centred at ~950 cm^{-1} (νSi–O modes in dangling oxygen atoms). As shown in Figure 5, this band was fitted by two Gaussians, at ~960 and ~900 cm^{-1}, assigned to the Si–OH and Si–O^- groups, respectively.[33] These groups are both hydrophilic, and so their proportion in the total silica network [$\%(Si–O_d)$] may be taken as a measure of the sample's hydrophilicity degree. It may be calculated by the following ratio of percentual areas [Eq. (13)]:

$$\%(Si-O_d) = 100 \times \frac{\%A(\nu Si-OH + \nu Si-O^-)}{\%A(\nu_{as} Si-O-Si + \nu Si-OH + \nu Si-O^-)} \quad (13)$$

The evolution of this percentage as a function of the molar ratio x, depicted in Figure 6, clearly shows that a slight decrease in the hydrolysis pH is responsible for an exponential reduction in the proportion of surface hydrophilic groups. Below pH 1.36 ($x = 0.009$), no significant further decrease is foreseeable. This characteristic may be slightly improved by increasing y from 1 (sample HYD_3 or $COND_{10}$) to 1.3 ($COND_{13}$), which induces a decrease in $\%(Si–O_d)$ from 12 to 8% in the samples with $x = 0.003$. In conclusion, the best results in terms of the xerogels hydrophobicity will be attained for hydrolysis pH ~1.4 and NH_3/HCl ratio in the condensation step of ~1.3.

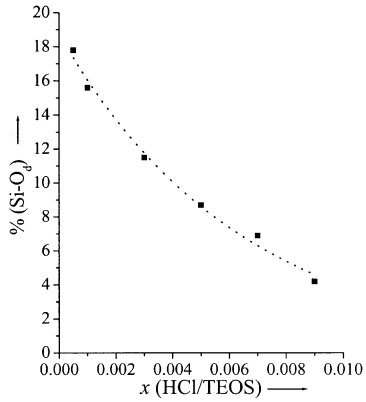

Figure 6. The evolution of $\%(Si–O_d)$ as a function of the molar ratio x.

Conclusions

By an efficient separation of the hydrolysis and condensation steps in the sol–gel process, through catalysis conditioning, it was possible to control individually the kinetics and mechanisms of each step. This allowed us to tailor the local structure of TEOS-based porous silica xerogels, as characterised by DRIFT spectroscopy. All the samples prepared are built upon a distribution of siloxane 6- and 4-rings, the latter being predominant, as would be expected for silica xerogels. However, the proportion of 6-rings may be increased (up to ~30%) upon increasing the HCl/TEOS ratio in the hydrolysis step and/or the NH_3/HCl ratio in the condensation step. Simultaneously, there is a decrease in the fraction of dangling oxygen atoms (unreacted silanol groups and broken Si–O–Si bridges), resulting in a certain degree of hydrophobicity and, therefore, in the chemical stability of the xerogels towards moisture. What is striking about these results is that these kinds of molecular changes (increase in the 6-rings and decrease in the dangling oxygen proportions) are usually observed upon the xerogels densification processes, but here it appears associated to an increase in the materials' porosity.

Acknowledgement

This work was funded by Fundação para a Ciência e a Tecnologia (FCT)—Project POCTI/CTM/33487/2000. A.F. is grateful to FCT for a PhD grant PRAXIS XXI/BD/19815/99.

[1] C. J. Brinker, G. W. Scherer, *Sol–Gel Science and Technology—The Physics and Chemistry of Sol–Gel Processing*, Academic Press, Boston, MA, **1990**.
[2] R. K. Iller, *The Chemistry of Silica*, Wiley, New York, **1979**.
[3] H. Schmidt, *J. Non-Cryst. Solids* **1988**, *100*, 51–64.
[4] C. J. Brinker, *J. Non-Cryst. Solids* **1988**, *100*, 31–50.

[5] B. E. Yoldas, *J. Am. Ceram. Soc.* **1982**, *65*, 387–393.
[6] B. E. Yoldas, M. J. Annen, J. Bostaph, *Chem. Mater.* **2000**, *12*, 2475–2484.
[7] A. Fidalgo, M. E. Rosa, L. M. Ilharco, *Chem. Mater.* **2003**, *15*, 2186–2192.
[8] C. J. Brinker, K. D. Keefer, D. W. Schaefer, C. S. Ashley, *J. Non-Cryst. Solids* **1982**, *48*,47–64.
[9] C. J. Brinker, K. D. Keefer, D. W. Schaefer, R. A. Assink, B. D. Kay, C. S. Ashley, *J. Non-Cryst. Solids* **1984**, *63*,45–59.
[10] E. Pope, J. Mackenzie, *J. Non-Cryst. Solids* **1986**, *87*,185–198.
[11] J. R. Martinez, F. Ruiz, Y. V. Vorobiev, F. Pérez-Robles, J. González-Hernández, *J. Chem. Phys.* **1998**, *109*, 7511–7514.
[12] A. Fidalgo, L. M. Ilharco, *J. Non-Cryst. Solids* **2001**, *283*, 144–154.
[13] A. Fidalgo, M. E. Rosa, L. M. Ilharco, in *Emerging Fields in Sol-Gel Science and Technology* (Eds.: T. M. Lopez, D. Avnir, M. Aegerter) Kluwer Academic, Boston, **2003**.
[14] P. N. Sen, M. F. Thorpe, *Phys. Rev. B* **1977**, *15*, 4030–4038.
[15] F. L. Galeener, *Phys. Rev. B* **1979**, *19*, 4292–4297.
[16] W. H. Zachariasen, *J. Am. Chem. Soc.* **1932**, *54*, 3841–3851.
[17] R. L. Mozzi, B. E. Warren, *J. Appl. Crystallogr.* **1969**, *2*, 164–172.
[18] M. F. Thorpe in *Vibrational Spectroscopy of Molecular Liquids and Solids* (Eds.: S. Bratos, R. M. Pick) Plenum, **1980** pp. 341–366.
[19] F. L. Galeener, M. F. Thorpe, *Phys. Rev. B* **1983**, *28*, 5802–5813.
[20] S. W. de Leeuw, H. He, M. F. Thorpe, *Solid State Commun.* **1985**, *56*, 343–346, and references therein.
[21] K. Kamiya, Y. Iwamoto, K. Yoko, S. Sakka, L. Hench, *J. Non-Cryst. Solids* **1988**, *100*, 195–200.
[22] J. K. West, L. L. Hench, B. Zhu, Y. C. Cheng, *J. Non-Cryst. Solids* **1990**, *121*, 51–55.
[23] F. L. Galeener, G. Lucovsky, *Phys. Rev. Lett.* **1976**, *37*, 1474–1478.
[24] M. F. Thorpe, S. W. de Leeuw, *Phys. Rev. B* **1986**, *33*, 8490–8505.
[25] J. C. Decius, R. M. Hexter, *Molecular Vibrations in Crystals*, McGraw–Hill, New York, **1977**.
[26] S. W. de Leeuw, M. F. Thorpe, *Phys. Rev. Lett.* **1985**, *55*, 2879–2882.
[27] P. Kubelka, F. Munk, *Z. Tech. Phys.* **1931**, *12*, 593–601.
[28] K. Kamiya, T. Yoko, K. Tanaka, M. Takeuchi, *J. Non-Cryst. Solids* **1990**, *121*, 182–187.
[29] H. Yoshino, K. Kamiya, H. Nasu, *J. Non-Cryst. Solids* **1990**, *126*, 68–78.
[30] S. Hayakawa, L. Hench, *J. Non-Cryst. Solids* **2000**, *262*, 264–270.
[31] J. C. G. Pereira, C. R. A. Catlow, G. D. Price, *J. Phys. Chem. A* **1999**, *103*, 3268–3284.
[32] K. Kamiya, A. Oka, H. Nasu, T. Hashimoto, *J. Sol–Gel Sci. Technol.* **2000**, *19*, 495–499.
[33] A. Chmel, E. K. Mazurina, V. S. Shashkin, *J. Non-Cryst. Solids* **1990**, *122*, 285–290.

Received: April 28, 2003
Revised: July 18, 2003 [F5079]